Huth Tyler (Orcid ID: 0000-0002-3436-7009)
Marchetti David, W. (Orcid ID: 0000-0002-1246-0798)
Bowling David, R. (Orcid ID: 0000-0002-3864-4042)

Seasonal bias in soil carbonate formation and its implications for interpreting high-resolution paleoarchives: evidence from southern Utah

Huth, T.E.[1*], Cerling, T.E.[1], Marchetti, D.W.[2], Bowling, D.R.[3], Ellwein, A.L.[4], and Passey, B.H.[5]

[1]*Department of Geology and Geophysics, University of Utah, Salt Lake City, UT 84112, USA*

[2]*Department of Natural and Environmental Sciences, Western State Colorado University, Gunnison, CO 81231, USA*

[3]*Department of Biology, University of Utah, Salt Lake City, UT 84112, USA*

[4]*Rocky Mountain Biological Laboratory, Crested Butte, CO 81224, USA*

[5]*Department of Earth and Environmental Sciences, University of Michigan, Ann Arbor, MI 48109, USA*

*Corresponding author

Email address: tyler.huth@utah.edu (T. Huth).

KEY POINTS

1. At Torrey, UT, comparison between modern soil and late Holocene soil carbonate isotopes shows soil carbonate forms during the summer.

This is the author manuscript accepted for publication and has undergone full peer review but has not been through the copyediting, typesetting, pagination and proofreading process, which may lead to differences between this version and the Version of Record. Please cite this article as doi: 10.1029/2018JG004496

2. Summer formation seasonality occurs because calcite dissolution-formation reactions during infiltration events overprint prior material.
3. Torrey soil carbonate rinds are suitable material for high-resolution paleorecords as proxies of summer soil and vegetation conditions.

ABSTRACT

Pedogenic carbonate is commonly used as a paleoarchive, but its interpretation is limited by our understanding of its formation conditions. We investigated laminated soil carbonate rinds as a high-resolution paleoarchive in Torrey, Utah, United States by characterizing and modeling their formation conditions. We compared late Holocene (<5 ka) soil carbonate conventional (C and O) and "clumped" isotopes to modern soil environment and isotope measurements: soil CO_2 partial pressure, soil temperature, soil moisture, δ^{13}C-soil CO_2, δ^{18}O-precipitation and δ^{18}O-soil water. Data unambiguously identified a strong summer seasonality bias, but modeling suggested soil carbonate formed several times throughout the year during infiltration events causing dissolution-formation reactions. This apparent discrepancy resulted from preferential preservation of calcite formed from the largest annual infiltration events (summer) overprinting previously formed calcite. Soil carbonate therefore formed predominantly due to changes in soil water content. As soil CO_2 was at its annual maximum during soil carbonate formation, assuming uniformly low soil CO_2 formation conditions for soil carbonate in estimating paleoatmospheric CO_2 is likely not viable. Additionally, we showed modern summer δ^{13}C-soil CO_2 and soil CO_2 measurements could not produce a modeled δ^{13}C-soil carbonate consistent with late Holocene observations. We suggest using multiple lines of evidence to identify non-analogous modern

conditions. Finally, a nearly linear radiocarbon age model from a laminated rind showed that rinds can be used as a high-resolution paleoarchive if samples are from a single depth and the timing and conditions of soil carbonate formation can be constrained through time.

1. INTRODUCTION

Pedogenic carbonate forms in semiarid and arid soils from the interaction between infiltrating water and a source of dissolved calcium. Calcium sources include dust and weathering of calcic and silicate parent material (Chadwick & Davis, 1990; McFadden et al., 1992; Reheis & Kihl, 1995). Regardless of the source, dissolved calcium ions travel in a soil with infiltrating water and are held on soil particles by surface tension until changes in ion activity (via ion exclusion through evaporation, transpiration and/or microorganisms), changes in the partial pressure of CO_2 (pCO_2, by biologic activity), and/or temperature cause saturation with respect to calcium carbonate (Cerling, 1984; Treadwell-Steitz & McFadden, 2000; Breeker et al., 2009; Zhu & Dittrich, 2016). Carbonate-bicarbonate equilibria is expressed as:

$$2HCO_3^-{}_{(aq)} + Ca^{2+}{}_{(aq)} \leftrightarrow CaCO_{3\,(s)} + CO_{2\,(g)} + H_2O_{\,(l)} \quad (1)$$

Understanding how this relationship changes under specific soil environment conditions is of considerable importance because the stable isotopes of C and O in pedogenic carbonate are related to biologic activity (C) and soil water (O) during the time of formation (Cerling, 1984; Cerling et al., 1989) and hence can act as a paleoarchive of climate and ecologic change. In theory, interpretation of a soil carbonate paleoarchive would rest on a site-specific understanding of (1) soil carbonate formation and

mechanisms, (2) the annual cycle of soil C- and O-isotopes, and (3) how formation times, formation mechanisms, and soil isotope cycling might change under different global climate conditions.

In practice, conceptual and quantitative models of soil carbonate dynamics are hindered by the inability to sufficiently characterize input parameters. For example, researchers have identified summer, the end of the growing season (i.e., timing of maximum plant activity), or springtime as the dominant season of pedogenic carbonate formation (Breeker et al., 2009; Gallagher & Sheldon, 2016; Oerter & Amundson, 2016; Quade et al., 2013; Ringham et al., 2016; Burgener et al., 2016; Peters et al., 2013). Temporally coarse field data resolution, lack of soil moisture and/or soil CO_2 data, and using annual vs. seasonal vegetation regimes all hinder studies of modern soil carbonate dynamics. In addition, while studies have avoided sites with obvious agricultural disturbance, it is difficult to address disturbance from grazing and species invasion. Grazing for example, can result in reduced grass and sedge biomass and density, compacted soils with reduced infiltration rates, and have feedback effects on fire regimes (Cole et al., 1997; Belsky & Blumenthal, 1997). Effects on soil carbonate dynamics are therefore possible, but difficult to constrain due to complex interactions between disturbances and, for example, local plant species, soil type, topography, the disturbances themselves, and changing land management practices (Chambers et al., 2016). Field methodologies are also generally unable to differentiate between single and multiple formation time periods. For example, soils may have similar isotopic profiles with depth during the spring and fall, which can make it difficult to distinguish if one or both are formation time periods. More recent work utilizes formation temperature estimates from clumped isotopes as an additional constraint (Quade et al., 2013), but this is not yet a routine measurement and can still yield non-unique results. Seasonality issues are especially critical in light of the potential for high-resolution

(100s yr) soil carbonate records, as demonstrated by pedogenic carbonate rinds from fluvial terraces in the Wind River Basin (Oerter et al., 2016) and archeological sites in the Fertile Cresent (Pustovoytov et al., 2007). These studies are intriguing because they suggest the possibility of long-term, sub-millenial soil carbonate archives that can be used to investigate Quaternary timescales for which only a few proxies are available.

In this study, we investigated the potential of laminated soil carbonate that occurs as rinds on large boulders near Torrey, Utah, United States to serve as a paleoclimate and paleoecology proxy. Our goals were to (1) date the laminated soil carbonate to assess the feasibility of the radiocarbon methodology in developing a chronology, (2) measure all relevant soil carbonate environmental parameters (soil CO_2, temperature, and soil moisture) and associated isotopic values to characterize the modern soil environment, (3) match modern observations to calcite chemistry to determine the dominant time(s) of calcite formation, and (4) model the yearly cycle of dissolved Ca^{2+} mass to provide a quantitative basis for understanding calcite formation.

2. STUDY LOCATION AND METHODOLOGY

2.1. Geologic setting

We studied soils developed on middle- to late Pleistocene geomorphic surfaces related to mass movement deposition the Fremont River Valley, near the town of Torrey in southern Utah, United States (Figure 1). The mass movements originated from Boulder and Thousand Lakes Mountains. On both sides of the valley they were the result of weak Jurassic to Eocene age sedimentary rocks failing and causing

the overlying ≈26 Ma Johnson Valley Reservoir trachyandesite (hereafter "andesite") to break off in sharp scarps and move as rotational slumps and translational landslides, later remobilizing as boulder debris flows (Marchetti et al., 2007; Marchetti et al., 2012; Bailey et al., 2007). These debris flow deposits are primarily composed of large (0.2 to > 1 m) andesite boulders within a finer-grained matrix of mixed sedimentary units (mudstone, limestone, sands, silts, chert pebbles, etc.). The dense andesite boulders stabilized the surfaces against erosion (Marchetti et al., 2012), which over time created an inverted topography that allows correlation of more than 20 different surfaces. Cosmogenic ^{3}He dates demonstrate that debris flow deposits range in age from ≈100 ka to over 1.4 Ma in the region (Marchetti, 2006; Marchetti et al., 2012). Soils developed on these debris flows have significant calcite accumulation (≥Stage III carbonate morphology as in Gile et al., 1996).

At Torrey, pedogenic carbonate formed in several morphologies. We focused on the carbonate rinds found on the bottom of large (>1 m b-axis) boulders as they formed in a stable position, have a deep formation depth (>40 cm), and have an identifiable stratigraphy useful for dating (Figure 2). We compared recent pedogenic carbonate with modern soil conditions at two similarly aged debris flow surfaces (Figure 1). The Teasdale Bench (TB - N 38.3002°, W 111.4788°) and Bench DH (DH - N 38.2706°, W 111.4087°) have similar elevations (≈2110 and 2080 masl, respectively), which suggests they had similar base levels and are of similar age. We used two benches because we necessarily had to break up portions of the pedogenic carbonate sampling and the modern monitoring. Part of the modern monitoring included measuring soil CO_2, which required a long-term, reliable source of power. Site DH is near a housing development that we used as a power source for our monitoring (Figure 1). Collecting pedogenic carbonate rinds from the same bench was problematic because the largest rinds in which we

are interested form on the bottoms of ≈1 m boulders that can only be accessed in situ with a backhoe. In addition, only about one in thirty pedogenic rinds appeared suitable for dating (i.e., had visually continuous stratigraphy), which meant we had to collect many samples for screening. It was not possible to trench DH to obtain samples, so we utilized a series of boulders and their rinds on TB that were excavated during highway construction (Figure 1).

2.2. Climate

Torrey, UT has a semiarid climate, receiving ≈260 mm of annual precipitation (Prism Climate Group, 2018). It sits on the northern edge of the region affected by the North American Monsoon (NAM) (Higgins et al., 1997) with 45 % of annual rainfall in JASO (Figure 1). This seasonal bias in meteoric precipitation may be enhanced by the site's location between mountain ranges to the north and south (Figure 1). Summer rain events occur in the mid- to late afternoon, are generally short in duration (1-3 hr) and supply 0.2-0.3 cm of rain (Capitol Reef National Park weather station; MesoWest, 2017). However, large events precipitating 0.5-1 cm of rain also occur. Temperature seasonality is strong at Torrey; average daily temperature (average low/high) in January and July are -3.7 °C (-11.3/3.9 °C) and 20.2 °C, (11.4/28.9 °C), respectively. Snowpack only lasts about a week to a month following snowfall events. Days with the largest rain and/or snow amounts occur January-March and August-October, which makes these the most likely times for rain to infiltrate into the deep soil.

2.3. Modern measurements

We measured modern environmental conditions to provide a baseline for understanding the timing of modern soil carbonate formation and the isotopic signature of resulting soil carbonate. The measured parameters were soil temperature, soil moisture, soil CO_2, $\delta^{13}C$-soil CO_2, $\delta^{18}O$-soil water, and $\delta^{18}O$-water (rain and snow). To understand soil carbonate dynamics, we additionally modeled calcite dynamics at 40 cm depth. We briefly describe the methods with a full accounting available in Supplementary Text S1.

2.3.1. Soil characterization

The soil at TB was characterized through soil stratigraphic techniques to place rinds in their in situ soil context. Stratigraphy was described via a 2 m deep, 5 m long trench (Figure 2). The trench site bordered a large boulder (≈1 m b-axis) to provide a situation analogous to our sampled rinds. Field soil descriptions included depth and thickness of soil horizons, horizon boundaries, Munsell soil color, texture, structure, consistence, and morphology of clay films, and pedogenic carbonate (Birkeland, 1999; Birkeland et al., 1991). Two field descriptions were taken, one next to the large boulder and the other away from it (hereafter near-boulder and no-boulder profiles; Supplementary Table 1).

2.3.2. Soil conditions

Temperature, soil moisture, and soil CO_2 were measured during the study to understand general seasonal trends (Figures 3C, 3D and 4; Supplementary Table 2). The TB and DH sites both had temperature measurements (TB 2014-2017, DH 2014-2015), while only DH had soil moisture and soil CO_2 measurements (2014-2015). Temperature and soil moisture measurements were taken every 15

minutes with HOBO loggers at 0-40 cm depth. Soil CO_2 samples were extracted from stainless steel gas wells (2 plots of 15-45 cm) and measured every 2 hours using a LI-COR LI-820 infrared gas analyzer connected to an automated pump system (similar to Bowling et al., 2015). Samples were calibrated to a tank of known pCO_2 or, where tank failure disallowed this, to the most recent ambient air CO_2 values. This extra introduced error is not significant for our purposes. Several data gaps in the CO_2 data occurred due to power loss and animal interference.

2.3.3. δ^{13}C-soil CO_2

Two sites on TB (TB1 and TB2) and one site on DH were sampled from 10-40 cm for δ^{13}C-soil CO_2 (TB1 and TB2 2015-2017, DH 2015; Figure 3A-3C) using stainless steel gas wells hammered into the ground, a VICI Pressure-Lok Precision Analytical Syringe, and Labco Exetainer gas-tight vials with rubber septa vacuumed to < 13.3 kPa in the field (Supplementary Table 3). Sampling periods after August 22, 2016 had two samples taken from each well to assess replicability and air samples were collected starting in September 2016. Most sample periods comprised a single day, but we performed two monitoring campaigns through rain events during summer 2015 with 2-3 sampling times per day over a 3-5 day period. Gas samples were measured within 24 hours of the final collection. Sample CO_2 was measured with a closed-loop LI-COR LI-7000 infrared gas analyzer and δ^{13}C was measured with continuous flow isotope ratio mass spectrometry (Thermo Finnigan Delta plus XL, University of Utah SIRFER laboratory). Samples have long term precision of ± 0.2 ‰ VPDB and were corrected via three internal lab standards (tanks 200089, 202353, and IF002531) calibrated against IAEA standards RM8562 and RM8563.

We identified the overall vegetation respiration signal (δ^{13}C-respiration; Figure 5A) by assuming diffusive gas transport dominated in the soil and calculating the best fit line to the data plotted as $1/CO_2$ vs. δ^{13}C-soil CO_2 (Cerling et al., 1991; Pendall et al., 2001). Sample periods without air samples were assigned the average air value during the study interval. The y-intercept (at 'infinite CO_2') is the δ^{13}C-respiration plus 4.4 ‰ VPDB due to the effects of diffusion. To allow comparison with modeled δ^{13}C-soil CO_2 required to create observed δ^{13}C-soil carbonate, all modern δ^{13}C-respiration values are reported with an additional +1.7 ‰ VPDB anthropogenic correction (total correction = -2.7 ‰ VPDB).

2.3.4. δ^{18}O-water and δ^{18}O-soil water

Water was collected from snow, rain, and soil to characterize the local meteoric water line and document seasonal variation (Figure 5B-5D; Supplementary Table 4). Seasonal precipitation was collected in a bottle containing mineral oil to inhibit evaporation. Snow was collected from Bench TB as well as from late-season snowpack on Boulder Mountain. In addition, individual rain events were opportunistically collected in person in the Fremont valley and nearby mountain ranges.

δ^{18}O-soil water was monitored at sites TB1 and TB2 (2016-2017; Figure 5B-5D; Supplementary Table 4). Torrey soils can be difficult to dig in due to the presence of large boulders so we dug to at least 40 cm, but preferably to 100 cm depth. The November 2016 collection was done from two 2 m deep backhoe trenches dug 10 m apart. February 2017 sampling was only to 40 cm due to difficulty digging at this time of year

All samples were collected in scintillation vials and immediately sealed with Parafilm. Pure waters were kept in a refrigerator until measurement and soils kept frozen until extraction on a vacuum

line and measurement. All water samples were measured via a Picarro L1102-i WS-CRDS Mass Spectrometer at the University of Utah SIRFER laboratory. SIRFER standards PZ, UT2, and EV were used and precision was ± 1.1 ‰ VSMOW and ± 0.15 ‰ VSMOW for δD and $\delta^{18}O$, respectively.

2.4. Soil carbonate rinds

Soil carbonate rinds were collected to compare the youngest material with modern environmental conditions.

2.4.1. Sample collection

Rinds were collected from the TB debris flow (Figure 1). We targeted large (≥ 1 m) boulders for samples because these provide stable growth surfaces for well-laminated, 1-2 cm thick rinds. However, as it was not possible to expose these boulders by hand, we utilized the boulder piles that lined a highway passing through the bench. Using large boulders also allowed us to estimate depth of formation and mitigate soil isotopic effects. Many boulders exhibited clear color transitions from aerial exposure with desert varnish, to a calcite leached zone, to a calcite accumulation zone with rinds formed between 40-60 cm (Figure 2, see Soil stratigraphy below). Rinds formed at >40 cm would not likely have experienced strong air-soil CO_2 isotopic mixing but do have potential to experience evaporative effects (Cerling, 1984; Cerling et al., 1989; Breeker et al., 2009; Oerter & Amundson, 2016).

Loss of rind calcite through exposure is not likely to be an important consideration for our goals here. Assuming that all Torrey rainfall interacted with an exposed rind, equilibrium (i.e., maximum) dissolution, and 100 years since overturning, ≈400 µm (≈2 ka) of rind would be dissolved. However, this

situation is unlikely as most water would immediately drain from the boulder surface and reaction kinetics would greatly inhibit dissolution. Therefore, calcite loss from exposure is not likely an important consideration.

2.4.2. Sample selection and milling

Rinds were cross-sectioned and examined visually and microscopically for continuous laminations (Figure 2B). The selected rind, Pendant 11-8, was chosen because of its continuous stratigraphy and few large void spaces. It was sampled by milling off thin (100 µm for radiocarbon, 33 µm for stable isotope analysis) sections of rind using an automated MicroMill system. This single rind was explored as preliminary work in developing it as a high-resolution paleorecord. Cutting lines were drawn following the observed microscopic stratigraphy. We then interpolated between these lines using a function in the MicroMill program to obtain the finer sample sizes (Figure 2C). A total of 10 stable isotope samples (i.e., the youngest material, to ≈330 µm) and 9 radiocarbon samples (to ≈3300 um) were milled along a rind width of ≈2 cm.

2.4.3. ^{14}C dating

Sample preparation was done at the University of Utah (CO_2 extraction) and the University of Arizona (graphitization). Several sub-samples, milled at 100 µm resolution, were combined to obtain approximately 10 mg of sample. CO_2 was then extracted and purified under vacuum and graphitized before AMS and $\delta^{13}C$ measurements at the Arizona AMS Laboratory. Radiocarbon ages were calibrated

using the CALIB 6.0 software with the IntCal09 calibration curve (Stuvier & Reimer, 1993; Reimer et al., 2009) (Table 1).

2.4.4. Cosmogenic ^{3}He dating

We added two samples to preexisting cosmogenic ^{3}He data for TB and processed three new samples for DH (Table 1). The sample selection methodology followed previous work in the area (Marchetti et al., 2007; Marchetti et al., 2012; Marchetti, 2006). All samples were analyzed for He isotopes at the University of Utah Dissolved and Noble Gas Laboratory and standardized against Yellowstone Park gas (MM) at 16.5 Ra, where Ra is the ^{3}He/^{4}He ratio in air (1.39 x 10^{-6}). Samples were corrected for non-cosmogenic ^{3}He using shielded andesite samples following Marchetti (2006). Resulting ages are minimum boulder surface exposure ages and assume no boulder erosion. Topographic and snow shielding effects are minimal at these sites and were not included. Ages were calculated using the previous version of the CRONUS-Earth Project online exposure age calculator (after Balco et al., 2008; including ^{3}He production rate data from Goehring et al., 2010, http://hess.ess.washington.edu/).

2.4.5. Stable isotope analyses

Ten soil carbonate subsamples were prepared and measured at the University of Utah (δ^{13}C-soil carbonate and δ^{18}O-soil carbonate, Table 2). Between 60 and 70 µg of sub-samples milled at 33 µm resolution were weighed into silver capsules. These were dried under vacuum at 200 °C for two hours before measurement on a common acid bath carbonate inlet system coupled to a Finnigan MAT252

stable isotope mass spectrometer. Long term precision for $\delta^{13}C$ is ± 0.1 ‰ VPDB and for $\delta^{18}O$ is ± 0.2 ‰ VSMOW.

2.4.6. Δ_{47} "clumped" isotope temperatures, T(Δ_{47})

Several samples of the youngest soil carbonate (<10 ka) from Pendant 11-8 were measured at Johns Hopkins University to derive temperature estimates during the time of carbonate formation, T(Δ_{47}) (Eiler, 2007; Ghosh et al., 2006). Carbonate samples and standards (8-10 mg) were acid-digested, purified, and measured on an automated system connected to a ThermoFinnigan MAT 253. Continual measurements of CO_2 gases with known $\delta^{13}C$ and $\delta^{18}O$ values equilibrated at 0 °C and 1000 °C (equilibrium CO_2 gases) were also made to observe instrument linearity and to generate an empirical transfer function, which allows for presenting data in an absolute reference frame (Dennis et al., 2011). All equilibrium CO_2 gases analyzed during this session were used in the normalization of data using a 'moving heated gas line' framework (Passey et al., 2010; Supplementary Table 5). For reference, we observed the following Δ_{47} values for carbonate standards analyzed during the same analytical session: NBS-19, 0.391 ± 0.011 ‰ (1 s, n = 21); HAF Carrara (a.k.a. YCM), 0.392 ± 0.010 ‰ (n = 19); 102-GC-AZ01, 0.697 ± 0.012 ‰ (n = 35).

2.5. Equilibrium model of Ca^{2+} mass

We modeled the mass of dissolved Ca^{2+} in equilibrium with calcite at 40 cm depth (mol Ca^{2+} m^{-3} soil) to identify the timing of soil carbonate formation from soil temperature, soil CO_2, and soil moisture

data. Therefore, times of decreasing Ca^{2+} mass are viable soil carbonate formation periods. Soil CO_2 and equilibrium constants (i.e., temperature) control [Ca^{2+}] as (Drever, 1988):

$$\boldsymbol{m_{Ca^{2+}}} = \sqrt[3]{\boldsymbol{P_{CO_2}} \frac{\boldsymbol{K_1 K_{cal} K_{CO_2}}}{\boldsymbol{4 K_2 \gamma_{Ca^{2+}} \gamma^2_{HCO_3^-}}}} \quad \textbf{(2)}$$

K_1, K_{cal}, K_{CO_2}, and K_2 are equilibrium constants for the dissolution of H_2CO_3, $CaCO_3$, CO_2, and bicarbonate in water respectively, γ_i is the activity coefficient of a species, and m is the concentration. Multiplying [Ca^{2+}] by soil water content (θ) gives the mass of Ca^{2+} (mol Ca^{2+} m^{-3} soil). Therefore, decreasing Ca^{2+} mass related to soil moisture changes may dominate changes caused by temperature and soil CO_2 because changing soil water content with ion exclusion directly controls Ca^{2+} mass.

At 40 cm depth, we considered two scenarios to demonstrate the effect of including soil moisture in soil carbonate accumulation: equilibrium Ca^{2+} mass as a function of temperature and soil CO_2 but with constant soil water content as well as Ca^{2+} mass as a function of temperature, soil CO_2, and changes in ion activity related to variable soil moisture inputs (Figure 6, Supplementary Text S2). We chose one year of data from August 2014-2015 to utilize all soil CO_2 data. Temperature and soil moisture data were averaged in two hour windows to match soil CO_2 data and then used to calculate [Ca^{2+}] (black x's) (Drever, 1988). The calculated values are missing significant parts of the spring and late summer when soil moisture changed because soil CO_2 data was unavailable. To allow for a full year of data, we fit a sinusoid to the soil CO_2 data (red circles) and recalculated [Ca^{2+}] for both scenarios. Model-data residuals for soil CO_2 were generally <1000 ppm, but modeled soil CO_2 underestimated summer observations by up to 2000 ppm. For the constant soil water content scenario, we multiplied [Ca^{2+}] by average measured soil water content to get Ca^{2+} mass. Both scenarios were parameterized with a factor

considering the saturation state of incoming water, loss of ions by infiltration, and ion exclusion processes, but note that exact values for these processes are less important than the overall patterns of change in Ca^{2+} mass (Supplementary Text S2).

3. RESULTS

3.1. Modern soil

3.1.1. Surface ages

Debris flows TB and DH gave similar minimum mean cosmogenic ^{3}He ages (± 1σ of mean) of 266 ± 45 ka (n=3) and 307 ± 12 ka (n=3), respectively (Table 1). Their similar ages, emplacement mechanism, and close proximity (≈7 km apart) means that their climatic, ecologic, and geologic influences were similar through time. Although debris flow DH may have been deposited during an interglacial period, (≈MIS 9, ≈330 ka Lisiecki & Raymo, 2005) when all uncertainties are included (analytical, production rate, geomorphic), we consider the sites' subsequently shared 270-300 kyr history more relevant to soil and vegetation development than the exact depositional age of each deposit. We therefore used the environmental data from the two sites as a single dataset to identify broad seasonal trends.

3.1.2. Soil stratigraphy

The stratigraphic section at TB comprised a diamict modified by eolian input and significant accumulation of calcite and gypsum (Figure 2D, Supplementary Table 1). The two profiles had similar

characteristics, but the near-boulder profile had boundaries 10-15 cm deeper than the no-boulder profile. The near surface (near-boulder 0-27 cm, no-boulder 0-20 cm) had significantly less gravel than deeper horizons (≈10 % vs. ≈80 %) and minimal calcite. The next layer had extensive calcite accumulation, exhibiting Stage III-IV carbonate horizons that were weakly to moderately platy (near-boulder 27-56 cm, no-boulder 20-41 cm). This was followed by a more weakly developed carbonate horizon (Stage II-III, near-boulder 56-71 cm, no-boulder 41-62 cm) where gypsum also began to accumulate. Gypsum accumulation dominated deeper in the soil (carbonate ≤ Stage I).

3.1.3. Environmental measurements at 40 cm

Soil temperature, soil CO_2, and soil moisture all exhibited strong seasonality (Figure 4). We focus here on the 40 cm depth results as the most analogous for rind formation conditions. Soil temperature varied between freezing conditions in winter to a high of ≈25 °C in the summer. The effects of diel temperature changes and rainfall events could be seen on short timescales. Diel temperature changes were on the order of 1 °C at 40 cm while the largest rainfall events cooled the soil by 2-3 °C at this depth.

Soil CO_2 at 40 cm showed a strong annual pattern between 1000 ppm in the winter and >5000 ppm during the summer. It was in phase with the temperature data but also correlated with increases in soil moisture, particularly during the summer. There were two fast, steep drops in soil CO_2 during September 2014 and August 2015 where soil CO_2 dropped by 80-90% to <1000 ppm. It is not clear if these drops represent displacement of soil gas with water or are artifacts of our CO_2 sampling setup clogging and giving spurious numbers, so we do not discuss these drops further.

Soil moisture at 40 cm shows that infiltration largely occurred during the late winter–spring and the mid- to late-summer. Late winter–spring infiltration from snowmelt occurred slowly (days to a week), possibly dependent on snowpack extent. In contrast, summer infiltration generally occurred in <1 hr. In both cases, there were usually 1-4 weeks between infiltration events, allowing for substantial soil dewatering. Summer 2014 had two large 'monsoonal' rain events, while summer 2015 had two small infiltration events reaching 40 cm soil depth. Both years, however, had similar summer soil CO_2 levels.

Comparing our data with air temperature and rainfall from the nearest weather station outside of Capitol Reef National Park (CRNP, 20 km distant, 1650 masl ; MesoWest, 2017) suggests that the overall seasonal patterns at Torrey were representative of regional climate. At CRNP, total summer (JASO) and annual rainfall in 2015 were greater than in 2014. If this rainfall pattern is transferrable to Torrey, then larger rainfall event size may have produced the infiltration events in summer 2014. Regardless of site-specific conditions, our data likely captured the seasonal timing of changes, so we focus on this information to understand soil carbonate dynamics.

3.1.4. $\delta^{13}C$-respiration

$\delta^{13}C$-respiration exhibited strong seasonality (Figure 5A). Torrey's summer vegetation signal was -16 to -20.5 ‰ VPDB, while winter was -23 to -25 ‰ VPDB. Pre-industrial plants using the C_3 and C_4 photosynthetic pathways have average isotopic compositions of -24 ‰ and -10 ‰ VPDB, respectively (Cerling & Harris, 1999; Tipple & Pagani, 2007). However, C_3 plants living in water-stressed conditions incorporate relatively more ^{13}C than well-watered counterparts, while C_4 plants maintain a relatively constant discrimination (Cerling & Harris, 1999). Therefore, for summer months a preindustrial C_3

endmember is more likely to be -24 to -22 ‰ VPDB while the C_4 endmember remains -10 ‰ VPDB (Ehleringer & Monson, 1993). These data were therefore consistent with dominantly C_3 photosynthetic activity during the winter and C_3+C_4+CAM photosynthetic activity during the summer.

3.1.5. δ^{18}O-water and soil water

The δ^{18}O-rainwater data varied from ≈0 ‰ VSMOW in the summer to -18 ‰ VSMOW in the winter (Figure 5B). The small individual rain events sampled during the summer were especially evaporated (+1 to -5 ‰ VSMOW). The larger rain events that could penetrate to >40 cm likely had δ^{18}O values closer to (or even more negative) than -5 ‰ VSMOW.

Soil water δ^{18}O data showed roughly sinusoidal variability that was coherent within three differing zones of activity at about 0-20, 20-40, and >40 cm depth based on the no-boulder soil stratigraphy (Figure 5B; Supplementary Table 1). The 0-20 cm fraction ranged from -5 to +6 ‰ VSMOW, the 20-40 cm fraction ranged from -6 and -2 ‰ VSMOW, and the >40 cm fraction ranged from -11 and -3 ‰ VSMOW. However, while the 0-20 and >40 cm fractions had their minimum values in winter and maximum in summer, the 20-40 cm fraction had its maximum in winter and minimum in summer. Soil waters, including those down to 100 cm depth, all plotted to the right of the Local Meteoric Water Line (LMWL, Figure 5C and 5D) except for one anomalous value in the 20-40 cm fraction. Samples shallower than 20 cm tended to fall further from the LMWL than near surface samples, but there was little difference between samples deeper than 20 cm.

3.2. Soil carbonate

3.2.1. Radiocarbon dates, stable isotopes, and "clumped" isotopes.

Radiocarbon dates were in stratigraphic order and exhibited a nearly linear growth rate (r^2 = 0.97, n = 9, Table 1; Supplemental Figure 1). They spanned ≈6-18 cal ka BP and gave an extrapolated minimum age for the stable isotope samples of 2.7-4.3 cal ka BP. The ten carbonate stable isotope samples had δ^{13}C-soil carbonate ranging from -1.3 to -0.4 ‰ VPDB and δ^{18}O-soil carbonate ranging from -8.8 to -8.3 ‰ VPDB. δ^{13}C-soil carbonate averaged -0.6 ± 0.3 ‰ VPDB (1 σ) while δ^{18}O-soil carbonate averaged -8.6 ± 0.1 ‰ VSMOW (Table 2). The aggregate carbonate clumped isotope value (Δ_{47}) for the Holocene soil carbonate was 0.700 ± 0.009‰ (1 σ, 0.082‰ acid fractionation correction, Table 2). The calibrated Holocene soil carbonate formation temperature was calculated to be 24 ± 4 °C (95% confidence interval) based on the inorganic calcite calibration of Defliese et al., 2015, and this warm temperature was persistent regardless of chosen calibration (Table 2). Stable isotope values measured conventionally and for the youngest Δ_{47}-soil carbonate (D-025) were different, on average, by 0.4 (δ^{13}C) and 0.5 (δ^{18}O) ‰ VPDB, which may be the result of small-scale sample heterogeneity the milling technique could not resolve.

3.3. Equilibrium model of Ca^{2+} mass

The two model scenarios predicted qualitatively different soil carbonate formation times (i.e., times when Ca^{2+} mass decreased; Figure 6). Calculated Ca^{2+} mass as a function of temperature and soil CO_2 but constant soil moisture (e.g., Breeker et al., 2009) showed the late fall to winter as the dominant time of calcite formation, with another smaller event in the early summer. Weighting calculated Ca^{2+}

mass with variable soil moisture content showed instead that soil carbonate formed four times during the late winter-early spring and summer after infiltration events (dissolution-formation reactions; Figure 6). The summer formation events were substantially larger than the late winter-early spring events.

4. DISCUSSION

4.1. Soil stratigraphy constraints

The lack of gravel in surface horizons as compared to deeper horizons (≈10 % vs. 50-80 %) was consistent with soil inflation via eolian input. The soils also exhibited secondary mineral accumulations consistent with their age (≥ 265 ka) and the semi-arid setting (McFadden, 2013). Calcium is available in the parent material that makes up this soil, but the substantial eolian component in the upper soil means dust is likely the dominant calcium source at present. The 10-15 cm deeper horizon boundaries in the near-boulder profile may be caused by water moving preferentially along boulder-clast contacts. The soil horizons are also consistent with the color changes observed on exposed boulders and support our minimum depth estimate for rind formation via boulder size.

4.2. Timing and mechanism of soil carbonate formation

4.2.1. Comparison of $T(\Delta_{47})$ and modeled Ca^{2+} mass

Regardless of the calibration, Holocene soil carbonate formation temperatures were only consistent with modern soil temperatures during the summer (JJAS; Figure 4; Table 3) and were

inconsistent with freezing as a soil carbonate formation mechanism. The equilibrium Ca^{2+} mass model with constant soil moisture suggested a fall-winter formation time inconsistent with $T(\Delta_{47})$ data (Figure 6). In contrast, while the equilibrium Ca^{2+} mass model including variable soil moisture allowed for summer calcite formation, it also allowed for formation in the late winter-spring after each infiltration event. These ideas can be reconciled by recognizing that the largest dissolution-formation events will dominate observed rind seasonality. In addition to producing new material, each infiltration event will overprint older soil carbonate under contemporary conditions. The fluxes of soil carbonate dissolution-formation are therefore large compared to the total yearly accumulation (see calcite accumulation estimate in Supplementary Text S2). In such a system the season with the largest infiltration events, summer at Torrey, will dominate the observed soil carbonate seasonality by preferential preservation.

Other workers have also inferred the overarching importance of soil moisture in soil carbonate formation. Variable $T(\Delta_{47})$ in soil carbonates of the western United States across a range of precipitation regimes and soil types were interpreted as the result of differences in the timing of soil moisture depletion (Gallagher & Sheldon, 2016), but support for the interpreted mechanism was limited by a lack of in situ monitoring. Others have suggested carbonate formation during the wet season as the soil dries after rain events (Hough et al., 2014; Snell et al., 2013), during the driest part of the year (Breeker et al. 2009), or with significant variability due to elevation-driven climate differences (Oerter & Amundson, 2016). Our dataset builds on this previous work by demonstrating that (a) the timing of changes in soil moisture can be the predominant forcing for soil carbonate formation, (b) soil type and age may be important for the timing of soil carbonate formation because of the effects of developing vegetation

regimes and soil horizons, and (c) strong seasonal bias in soil carbonate isotope composition can develop in spite of multiple formation events each year as a result of preferential preservation.

4.3. Relationship between soil environment, soil isotopes, and soil carbonate

4.3.1. The relationship of soil CO_2 and $\delta^{13}C$-soil water to $\delta^{13}C$-soil carbonate

The pCO_2 and $\delta^{13}C$-respiration data were consistent with a mixed C_3-C_4-CAM landscape in the presence of a warm, wet growing season (Figures 4 and 5A). If modeled as a C_3-C_4 environment, winter values indicated a pure C_3 respiratory signal and summer values indicated a 30-50% C_4 contribution depending on the endmember value used for C_3 vegetation (-24 to -22 ‰ VPDB). The observed seasonal cycle was in contrast with other observations of maximum plant activity and belowground $\delta^{13}C$-soil CO_2 in southeastern Utah. Maximum plant activity at Corral Pocket on the UT-CO border was observed in the spring (Bowling et al., 2010). In addition, no seasonal cycle was observed in the $\delta^{13}C$-respiration of southeastern UT mixed C_3-C_4 grasslands (Bowling et al., 2011). These discrepancies may be due to a larger monsoonal influence at Torrey enhanced by the mountains to the north and south.

The $\delta^{13}C$-respiration values required to make observed $\delta^{13}C$-soil carbonate ranged from -13.3 to -14.7 ‰ VPDB using a diffusion-dominated soil model (temperature 18-30 °C, respiration 1-3 $mmol/m^2/hr$ = 3000-8000 ppm at 40 cm; Figure 5; Cerling, 1984; Cerling et al., 1989; Romanek et al., 1992; Solomon & Cerling, 1987). This range was 1-3 ‰ VPDB higher than the most enriched modern observation of -16 ‰ VPDB. Significant changes in soil respiration rate in the last ≈3 ka are unlikely to have caused the mismatch because they would need to be unreasonably large (an order of magnitude

lower). Instead, we interpret this mismatch as due to a recent change in the regional ecosystem like the late Holocene arrival of modern vegetation in the western US (Holmgren et al., 2007; Coats et al., 2008) or grazing and invasive species introduction (Belnap & Phillips, 2001). In any event, the annual cycle of δ^{13}C-respiration was qualitatively consistent with summer soil carbonate formation because the most enriched values occurred during the summer.

4.3.2. The relationship of soil water and δ^{18}O-soil water to δ^{18}O-soil carbonate

The δ^{18}O-soil water at Torrey represented a complex interplay between seasonal δ^{18}O-precipitation cycling, rain event size, freeze-thaw events, and evaporation. While infiltration of new water with seasonally variable δ^{18}O was evident (Figure 5B), δ^{18}O-soil water was strongly modified by evaporation (Figure 5C and 5D). This observation is in line with other studies from the western US suggesting that evaporation is an important factor even at depths >50 cm (Oerter & Amundson, 2016; Breeker et al., 2009). Other factors may also have been involved in the inversions of δ^{18}O-soil water data (Figure 5B). For example, in February 2017, freezing may have caused the isotopic inversion of the 0-20 and 20-40 cm fractions (-4 and -2.5 ‰ VSMOW, respectively). In addition, the inversion of the 20-40 and >40 cm fractions in summer 2017 and the datum to the left of the LMWL may have been caused by an upward water flux from >40 cm due to intense evapotranspiration and capillary wicking within the calcite horizon (e.g., Meyer et al., 2014).

The calculated δ^{18}O-soil water from which the soil carbonate formed was -8.6 to -5.1 ‰ VSMOW (Kim & O'Neil, 1997), consistent with the early summer >40 cm modern observations (Figure 5). We recognize that spring δ^{18}O-soil water >40 cm, which this dataset lacks, may also potentially match

calculated soil carbonate formation waters, but spring formation temperatures were inconsistent with soil carbonate T(Δ_{47}) and spring formation was therefore disregarded. Note that similar δ^{18}O-soil water values could be produced via summer rainfall and would be indistinguishable from δ^{18}O-soil carbonate data alone.

4.4. Broader implications

4.4.1. Implications for calibration studies

Calibration studies of soil carbonate must collect field data at high temporal resolution (e.g., Bowling et al., 2015; Oerter et al., 2017; Oerter & Bowen, 2017) and use several lines of evidence to identify formation times. For example, consider if the present dataset did not include high resolution environmental data. Without the environmental data, we could have concluded that soil carbonate formed only during (non-existent) extremely low pCO_2 and soil moisture conditions required for exceptionally high δ^{13}C-soil CO_2 values. More thorough monitoring systems including CO_2 measurements (e.g., Burgener et al., 2016) might help identify non-analogous conditions that may be responsible for modern data-to-soil carbonate mismatches (e.g., this study, Oerter & Amundson, 2016). Calibration studies should also carefully consider the spatial variability of soils as measurements of δ^{18}O-soil water at Torrey showed 2-3 ‰ variability within a small depth range on a single day (Gazis & Feng, 2004).

4.4.2. Implications for soil carbonate interpretation

Recent studies of the formation conditions of soil carbonate have emphasized the role that low soil CO_2 (Breecker et al., 2009b; Oerter & Amundson, 2016) may play in soil carbonate formation and its C-isotope composition. Our results suggest that these conditions are not ubiquitous. We agree that consideration of soil CO_2 concentration in interpreting δ^{13}C-soil carbonate is critical, but emphasize that uniformly assuming low soil CO_2 conditions during soil carbonate formation (Breecker et al., 2009a) has the potential to underestimate modeled atmospheric CO_2.

In addition, studies must consider the effects of multiple formation times on bulk soil carbonate isotope composition (Burgener et al., 2016). Studies regularly, and not necessarily incorrectly, assume that soil carbonate only forms at one time of the year (Gallagher & Sheldon, 2016; Breeker et al., 2009; Oerter & Amundson, 2016), but our data also suggest that the potential for mixed signals from multiple events throughout the year exists. Although summer conditions are dominantly preserved at Torrey today, changes in climate could feasibly produce soil carbonate produced from roughly equal parts winter and summer infiltration. Soil carbonate isotope composition would be indistinguishable from late spring soil conditions even though the material contained no information from that time period. Further study is needed of soils with multiple soil carbonate formation times and how the signal is isotopically recorded.

4.4.2. Implications for laminated soil carbonate paleorecords

This study also has implications for the use of laminated soil carbonate rinds as high-resolution proxies for late Quaternary paleoclimate and ecosystem changes. Similar to the age models from the two published records (Pustovoytov et al., 2007; Oerter et al., 2016), radiometric dating at Torrey

indicates laminated soil carbonates can be reliably dated. However, our results also highlight the utility of knowing the depth of formation as well as having extensive modern calibration data for interpreting soil carbonate formation conditions (Oerter & Amundson, 2016; Breeker et al., 2009; Burgener et al., 2016; Gallagher & Sheldon, 2016; Peters et al., 2013). Combining information on rinds from different depths (Oerter et al., 2016) is likely to obscure signals due to different infiltration, soil CO_2, and temperature regimes (Burgener et al., 2016; Peters et al., 2013; Quade et al., 2013). In addition, the seasonality and mechanism of soil carbonate formation will need to be addressed through the duration of these records (e.g., with $T(\Delta_{47})$ or other proxy information).

5. CONCLUSIONS

Soil carbonate formation at Torrey, UT occurred as the result of infiltration events in the late-winter–spring and the mid- to late-summer. The summer (NAM) infiltration events were larger and therefore overprinted other events, preserving an isotope composition dominantly reflecting summer soil conditions. Some lines of evidence (δ^{18}O-soil water, δ^{13}C-respiration) were ambiguous on their own. Soil carbonate δ^{13}C reflected summer vegetation composition while δ^{18}O reflected summer soil conditions resulting from infiltration seasonality, temperature, evaporation intensity, and changes in δ^{18}O-precipitation. Consequently, we inferred that:

(1) Multiple lines of evidence demonstrated non-analogous conditions for modern-late Holocene soil carbon isotopes at a field site that, while never tilled, may have been affected by other anthropogenic impacts or recent ecosystem change. Calibration studies of soil carbonate formation may suffer from

interpretations made between non-analogous modern conditions and soil carbonate formed over 100-1000s yr.

(2) Soil carbonate formation at Torrey dominantly responded to changing soil moisture conditions and formed during maximum annual soil CO_2 conditions (>3000 ppm). Assumptions of uniformly low soil CO_2 formation conditions in estimating paleoatmospheric CO_2 may not be viable.

(3) Soil carbonate could form multiple times during the year but showed a strong seasonal bias reflecting the balance of preservation of material from multiple dissolution-formation events. Soil carbonate studies must identify and account for this effect in interpretations.

(4) Laminated soil carbonate rinds can be used as high-resolution proxies for late Quaternary paleoclimate and ecosystem change if a suitable age model is demonstrated, analyses are made on a sample from a single depth, and the timing and conditions of soil carbonate formation can be constrained through time.

6. ACKNOWLEDGEMENTS AND DATA

This work was supported by NSF grants (Nos. 1325214, and 1325225) to Cerling, Marchetti, and Ellwein, a GSA Cole award to Marchetti, and by the following grants to Huth: NSF grant No. 1137336, University of Utah Geology and Geophysics grants, and a University of Utah Global Change and Sustainability Center grant. The authors wish to thank Dana Carroll and Jeannine Marlowe for allowing us to use their property and Austen Beason and Amy Allbritton for their assistance in the field and laboratory. Soil environmental and isotopic data can be found in the Supporting Information. The authors declare no conflict of interest.

TABLES AND CAPTIONS

TABLE 1: DATING RESULTS

^{14}C RESULTS FOR PENDANT 11-8

Sample #	AMS#	Sample material	Start distance from rind edge (μm)	End distance from rind edge (μm)	$\delta^{13}C$	Fmc[a]	^{14}C age (yr BP)	2-sigma calibrated range - low (cal yr BP)	2-sigma calibrated range - high (cal yr BP)	Mean age (calendar yrs BP)[b]		Linear age-model statistics	
14C-2016-002	AA108132	soil carbonate powder	0	800	-0.4	0.5479	5050	5740	5920	5810		slope	5.06
14C-2016-003	AA108133	soil carbonate powder	800	1100	-1.0	0.4485	6670	7490	7570	7540		intercept	2569
14C-2016-004	AA108134	soil carbonate powder	1100	1400	-1.5	0.4090	7420	8190	8330	8250		r^2	0.97
14C-2016-005	AA108135	soil carbonate powder	1400	1700	-2.8	0.3580	8500	9450	9590	9480			
14C-2016-006	AA108136	soil carbonate powder	1700	2000	-3.7	0.3087	9710	11120	11240	11160			
14C-2016-007	AA108137	soil carbonate powder	2000	2300	-3.9	0.2648	10960	12650	12880	12830			
14C-2016-009	AA108138	soil carbonate powder	2300	2600	-3.2	0.2064	13000	15340	15790	15540			
14C-2016-014	AA108604	soil carbonate powder	2600	2900	-2.5	0.1744	14030	16830	17310	17030			
14C-2016-015	AA108605	soil carbonate powder	2900	3200	-2.3	0.1500	15241	18360	18670	18510			

SAMPLING AND HELIUM ISOTOPE DATA FOR EXPOSURE-AGE SAMPLES

Location and sample number	Latitude (°N)	Longitude (°W)	Elevation (m asl)	Boulder height/ longest axis (m)	Sample thickness (cm)	Topo shielding factor	$^{4}He_{tot}$ (10^{12} atoms g^{-1})	$^{3}He_{tot}$ (10^{6} atoms g^{-1})	$^{3}He/^{4}He$ fusion	$^{3}He_{c}$ (10^{6} atoms g^{-1})[d]	$^{3}He_{c}$ uncertainty (10^{6} atoms g^{-1})	$^{3}He_{c}$ (%)	exposure age[e] (ka)	internal uncertainty (ka)
Teasdale Bench (TB)														
Cosmo_2015_001	38.29810	111.47982	2151	0.8/1.9	4	1.00	10.65	147.1	1.38E-05	143.0	6.9	97.2	240	12
Cosmo_2015_002	38.29848	111.47899	2151	1.1/2.1	2	1.00	24.87	203.6	8.19E-06	194.6	8.2	95.6	318	13
TB-03 (Marchetti, 2006)	38.29027	111.41434	2163	0.9/1.6	4	1.00	19.20	149.4	7.78E-06	145.4	7.5	97.3	241	13
										average age +/- 1σ			**266**	**45**
Bench DH (DH)														
Cosmo_2015_003	38.29125	111.41286	2081	1.0/1.9	2	1.00	23.22	185.5	7.99E-06	177.5	6.9	95.7	304	12
Cosmo_2015-004	38.29127	111.41282	2081	0.9/1.8	2	1.00	29.96	196.2	6.55E-06	187.1	8.4	95.3	321	15
Cosmo_2015_005	38.29027	111.41434	2077	0.9/2.1	3	1.00	21.96	180.0	8.20E-06	170.7	8.0	94.8	297	14
										average age +/- 1σ			**307**	**12**

[a]Fmc is fraction modern carbon and includes lab blank correction (specific to each run, or running average).

[b]Calendar years calibrated with CALIB 6.0 - Intcal 09, years BP (before present-1950 AD) at 2σ or full range if 2σ estimate not made at 95% confidence

[c]See text for how distance was calculated for these samples

[d]Cosmogenic $^{3}He_{c}$ determined from $^{3}He_{c} = {}^{3}He_{tot} - ({}^{4}He_{tot} * {}^{3}He/{}^{4}He$ shielded) where the $^{3}He/^{4}He$ shielded value is 2.078×10^{-7} (Marchetti, 2006)

[e]Exposure ages determined using the former CRONUS-Earth Project online exposure age calculator (http://hess.ess.washington.edu/)(after Balco et al., 2008) and given using the LSDn scaling routine (Lifton et al., 20

Table 1: Radiocarbon and cosmogenic ^{3}He dating results

TABLE 2: SOIL CARBONATE STABLE ISOTOPE DATA									
CONVENTIONAL STABLE ISOTOPE DATA									
Sample	$\delta^{13}C$ (VPDB)	$\delta^{18}O$ (VPDB)	Start distance from rind edge (µm)	End distance from rind edge (µm)	Age (cal kyr BP)				
S-001	-0.5	-8.8	0	33	2.7				
S-002	-0.6	-8.4	33	66	2.8				
S-003	-0.5	-8.6	66	99	3.0				
S-005	-0.7	-8.7	132	165	3.3				
S-006	-0.5	-8.7	165	198	3.5				
S-007	-0.5	-8.8	198	231	3.7				
S-008	-0.4	-8.7	231	264	3.8				
S-009	-0.4	-8.5	264	297	4.0				
S-010	-0.7	-8.3	297	330	4.2				
S-011	-1.3	-8.6	330	363	4.3				
average	-0.6	-8.6							
stdev	0.3	0.1							
ISOTOPOLOGUE DATA									
Sample	Start distance from rind edge (µm)	End distance from rind edge (µm)	Age (cal kyr BP)	n	$\delta^{13}C$ (VPDB)	$\delta^{18}O$ (VPDB)	Δ_{47}	1s	95% CI
D-025	0	400	3.6	3	-1.0	-9.0	0.700	0.011	0.013
D-026	400	800	5.6	1	-3.1	-9.3	0.702	0.007	0.013
D-027	800	1200	7.6	1	-3.5	-9.4	0.709	0.014	0.027
D-028	1200	1600	9.7	1	-3.3	-9.3	0.688	0.012	0.024
	overall				T (°C)[a]	T (°C)[b]	T (°C)[c]	T (°C)[d]	
	n	6		T_{avg}	24	20	22	24	
	$\Delta_{47\text{-weighted avg}}$	0.700		T_{low} (95% CI)	20	17	20	20	
	error (95% CI)	0.009		T_{high} (95% CI)	27	22	25	27	
[a]Temperature calculated from Defliese et al., 2015									
[b]Temperature calculated from Bonifacie et al., 2017									
[c]Temperature calculated from Passey and Henkes, 2012									
[d]Temperature calculated from Henkes et al., 2013									

Table 2: Soil carbonate conventional and "clumped" stable isotope data

FIGURE CAPTIONS

Figure 1: Overview of the Fremont Valley showing rind collection site and gas wells TB1 and TB2 (yellow star), gas well site D (red star), and $\delta^{18}O$ soil water collection sites, including the trench in Figure 2d (blue square). Inset in top left is a topographic map of Utah with a dashed line approximating the limit of the Colorado Plateau and a star denoting Torrey. The Teasdale Bench, Bench DH, and their associated cosmogenic ^{3}He ages are outlined by dashed black lines where they are least disrupted by anthropogenic activity. Thousand Lakes Mountain is to the north in this image (not visible) and Boulder Mountain is in the south of the image. Inset in bottom left shows Torrey region interpolated PRISM 30 year climate normal with precipitation (blue bar graph) and temperature (red line). Image is from Google Earth Pro.

Figure 2: Carbonate rind overview. (a) Boulder overturned during road construction near Teasdale Junction, Utah. Boulder surface color indicates soil horizons from when the boulder was in the ground (see text). (b) Cross section of Pendant 11-8 that formed on the bottom of a boulder. (c) Schematic view of how Pendant 11-8 was milled. (d) View to north of the trench on TB dug for soil descriptions. Pink ribbons outline the identified soil horizons, with the near-boulder profile on the left and the no-boulder profile on the right. Measuring tape is marked in 10 cm increments.

Figure 3: Torrey monitoring sites. Gas wells (yellow stars) for $\delta^{13}C\text{-}CO_2$ at (a) site TB1 and (b) site TB2. Walking path is denoted by the red arrows. Scale is the same for (a) and (b). (c) Environmental monitoring equipment at site DH. Grey box is the CO_2 autosampler and the white disturbed patch of

ground is the refilled access pit (yellow box). Gas wells are 2 m to the left of the tree (red box). Disturbed ground limit is denoted by the black dashed line. (d) Close-up of the refilled access pit in (c). Soil gas sampling sites are numbered. Wells 1-4 are 10-40 cm (1 = 10 cm) and this is repeated on the other side of the pit in wells 6-8. Temperature monitors are labeled 'T#' and soil moisture monitors are labeled 'SM#'. Numbers 1-4 for these monitor sets are 10-40 cm.

Figure 4: Soil environment data from site DH, north side. Only the deepest data (≈40 cm) is shown for clarity. Soil air CO_2 is on top, temperature is in the middle and soil moisture is on the bottom. The clumped isotope formation temperature for soil carbonate is outlined by the red dashed lines. Soil moisture is on a log scale to show smaller infiltration events.

Figure 5: Torrey soil and meteoric isotopes. (a) $\delta^{13}C$-respiration (accounts for -4.4 ‰ diffusion effect and 1.7 ‰ anthropogenic greenhouse effect, see text) through time at sites TB1, TB2, and DH. The black dashed lines are the range of modeled $\delta^{13}C$-respiration values derived from observed $\delta^{13}C$-soil carbonate under summer soil conditions. (b) Torrey $\delta^{18}O$ from snow (blue circles), individual rain events (open blue diamonds), long-term precipitation (open blue diamonds, bars indicate duration of collection), soil water from 0-20, 20-40, and >40 cm (yellow circles, green x's, and red circles; lines track average values), and the calculated $\delta^{18}O$-soil water for soil carbonate (black dashed lines). The anomalously low value from June, 20-40 cm depth is not included in the average (see text). (c) Torrey $\delta^{18}O$-soil water and rain samples as in plot (b) plotted against the Global Meteoric Water Line (black line;

Sharp, 2007) and the LMWL (open blue diamonds from rain samples, blue line is linear regression). (d) Torrey $\delta^{18}O$-soil water from >40 cm and the LMWL with time progressing from black to white.

Figure 6: Data compiled as day of year (DOY) and calculated mass of Ca^{2+} with and without variable soil moisture (see text). From top to bottom: soil moisture, soil temperature, soil CO_2, $\delta^{13}C$-respiration, $\delta^{18}O$-precipitation, calculated Ca^{2+} mass from soil temperature and soil CO_2 in a constant soil moisture regime, and calculated Ca^{2+} mass from soil temperature, soil CO_2, and variable soil moisture. Colored arrows on bottom two plots denote formation and dissolution events interpreted from the direction of Ca^{2+} mass change (see text). Black x's represent data and calculations from when soil CO_2 data was available while red circles represent modeled data and calculations based on a sinusoid fit to soil CO_2 data. Isotopic data from soil CO_2, rainwater, and soil water are fit with a sinusoid as a guide to the respective annual cycles. Vertical blue lines indicate start of infiltration events in soil moisture data.

REFERENCES

Bailey, C. M., Marchetti, D. W. & Harris, M. S., 2007. Geology and landscape history of the Fish Lake Plateau, Utah. In: W. R. Lund, ed. *Field Guide to Geologic Excursions in Southern Utah: Utah Geological Association Publication 35.* s.l.:Utah Geological Association, p. 25.

Balco, G., Stone, J. O., Lifton, N. & Dunai, T. J., 2008. A complete and easily accessible means of calculating surface exposure ages or erosion rates from ^{10}Be and ^{26}Al measurements. *Quaternary Geochronology,* Volume 3, pp. 174-195.

Belnap, J. & Phillips, S. L., 2001. Soil biota in an ungrazed grassland: Response to annual grass (Bromus tectorum) invasion. *Ecological Applications,* 11(5), pp. 1261-1275.

Belsky, A. J. & Blumenthal, D. M., 1997. Effects of livestock grazing on stand dynamics and soils in upland forests of the Interior West. *Conservation Biology,* 11(2), pp. 315-327.

Birkeland, P. W., 1999. *Soils and Geomorphology.* 3rd ed. New York City: Oxford University Press.

Birkeland, P. W., Machette, M. N. & Haller, K. M., 1991. Soils as a tool for applied Quaternary geology. *Utah Geological and Mineral Survey,* Volume Miscellaneous Publication 91-3, pp. 1-63.

Bonifacie, M. et al., 2017. Calibration of the dolomite clumped isotope thermometer from 25 to 350 °C, and implications for a universal calibration for all (Ca, Mg, Fe)CO_3 carbonates. *Geochimica et Cosmochimica Acta,* Volume 200, pp. 255-279.

Bowling, D. R. et al., 2010. Carbon, water, and energy fluxes in a semi-arid cold desert grassland during and following multi-year drought. *Journal of Geophysical Research,* Volume 115, pp. 1-16.

Bowling, D. R., Egan, J. E., Hall, S. J. & Risk, D. A., 2015. Environmental forcing does not induce diel or synoptic variation in carbon isotope content of forest soil respiration. *Biogeosciences Discussions,* Volume 12, pp. 6361-6404.

Bowling, D. R., Grote, E. E. & Belnap, J., 2011. Rain pulse response of soil CO_2 exchange by biological soil crusts. *Journal of Geophysical Research,* Volume 116.

Breecker, D. O., Sharp, Z. D. & McFadden, L. D., 2009a. Atmospheric CO_2 concentrations during ancient greenhouse climates were similar to those predicted for A.D. 2100. *Proceedings of the National Academy of Sciences,* Volume 107, pp. 576-580.

Breecker, D. O., Sharp, Z. D. & McFadden, L. D., 2009b. Seasonal bias in the formation and stable isotopic composition of pedogenic carbonate in modern soils from central New Mexico, USA. *Geol Soc Amer Bull,* Issue 121, pp. 630-640.

Burgener, L. et al., 2016. Variations in soil carbonate formation and seasonal bias over >4 km of relief in the western Andes (30°S) revealed by clumped isotope thermometry. *Earth and Planetary Science Letters,* Volume 441, pp. 188-199.

Cerling, T. E., 1984. The stable isotopic composition of modern soil carbonate and its relationship to climate. *Earth Planet Scie Lett,* Volume 71, pp. 229-240.

Cerling, T. E. & Harris, J. M., 1999. Carbon isotope fractionation between diet and bioapatite in ungulate mammals and implications for ecological and paleoecological studies. *Oecologia,* Issue 120, pp. 347-363.

Cerling, T. E., Solomon, D. K., Quade, J. & Bowman, J. R., 1991. On the isotopic composition of carbon in soil carbon dioxide. *Geochimica et Cosmochimica Acta,* Volume 55, pp. 3403-3405.

Cerling, T., Quade, J. & Bowman, J., 1989. Carbon isotopes in soils and paleosols as ecologic and paleoecologic indicators. *Nature,* Issue 341, pp. 138-139.

Chadwick, O. A. & Davis, J. O., 1990. Soil-forming intervals caused by eolian sediment pulses in the Lahontan basin, northwestern Nevada. *Geology,* Issue 18, pp. 243-246.

Chambers, J. C. et al., 2016. Plant Community Resistance to Invasion by Bromus Species: The Roles of Community Attributes, Bromus Interactions with Plant Communities and Bromus Traits. In: M. Germino, J. Chambers & C. Brown, eds. *Exotic Brome-Grasses in Arid and Semiarid Ecosystems of*

the Western U.S. Springer Series on Environmental Management. s.l.:Springer, Cham, pp. 275-303.

Coats, L. L., Cole, K. L. & Mead, J. I., 2008. 50,000 years of vegetation and climate history on the Colorado Plateau, Utah and Arizona, USA. *Quaternary Research,* Volume 70, pp. 322-338.

Cole, K. L., Henderson, N. & Shafer, D. S., 1997. Holocene vegetation and historic grazing impacts at Capitol Reef National Park reconstructed using packrat middens. *Great Basin Naturalist,* 57(4), pp. 315-326.

Defliese, W. F., Hren, M. T. & Lohmann, K. C., 2015. Compositional and temperature effects of phosphoric acid fractionation on Δ_{47} analysis and implications for discrepant calibrations. *Chemical Geology,* Issue 396, pp. 51-60.

Deinlein, U. et al., 2014. Plant salt-tolerance mechanisms. *Trends in Plant Science,* 19(6), pp. 371-379.

Dennis, K. J. et al., 2011. Defining an absolute reference frame for 'clumped' isotope studies of CO2. *Geochimica et Cosmochimica Acta,* Volume 75, pp. 7117-7131.

Drever, J. I., 1988. *The Geochemistry of Natural Waters.* second edition ed. Englewood Cliffs, New Jersey: Prentice Hall.

Ehleringer, J. R. & Monson, R. K., 1993. Evolutionary and ecological aspects of photosynthetic pathway variation. *Annual Review of Ecology and Systematics,* Volume 24, pp. 411-439.

Eiler, J., 2007. "Clumped-isotope" geochemistry - The study of naturally-occurring, multiply-substituted isotopologues. *Earth and Planetary Science Letters,* Issue 262, pp. 309-327.

Gallagher, T. M. & Sheldon, N. D., 2016. Combining soil water balance and clumped isotopes to understand the nature and timing of pedogenic carbonate formation. *Chemical Geology,* Issue 435, pp. 79-91.

Gazis, C. & Feng, X., 2004. A stable isotope study of soil water: evidence for mixing and preferential flow paths. *Geoderma,* Issue 119, pp. 97-111.

Ghosh, P. et al., 2006. ^{13}C–^{18}O bonds in carbonate minerals: A new kind of paleothermometer. *Geochimica,* Volume 70, pp. 1439-1456.

Gile, L. H., Peterson, F. F. & Grossman, R. B., 1996. Morphological and genetic sequences of carbonate. *Morphological and genetic sequences of carbonate accumulation in desert soils,* Issue 101, pp. 347-360.

Goehring, B. M. et al., 2010. A reevaluation of in situ cosmogenic ^{3}He production rates. *Quaternary Geochronology,* Volume 5, pp. 410-418.

Henkes, G. A. et al., 2013. Carbonate clumped isotope compositions of modern marine mollusk and brachiopod shells. *Geochimica et Cosmochimica Acta,* Volume 106, pp. 307-325.

Higgins, R. W., Yao, Y. & Wang, X. L., 1997. Influence of the North American Monsoon system on the U.S. summer precipitation regime. *Journal of Climate,* Volume 10, pp. 2600-2622.

Holmgren, C. E., Norris, J. & Betancourt, J. L., 2007. Inferences about winter temperatures and summer precipitation from the Late Quaternary record of C_4 perennial grasses and C_3 desert shrubs in the northern Chihuahuan Desert. *Journal of Quaternary Science,* 22(2), pp. 141-161.

Hough, B. G., Fan, M. & Passey, B. H., 2014. Calibration of the clumped isotope geothermometer in soil carbonate in Wyoming and Nebraska, USA: Implications for paleoelevation and paleoclimate reconstruction. *Earth and Planetary Science Letters,* Volume 391, pp. 110-120.

Kim, S.-T. & O'Neil, J. R., 1997. Equilibrium and non-equilibrium oxygen isotope effects in synthetic carbonates. *Geochimica et Cosmochimica Acta,* 61(16), pp. 3461-3475.

Klappa, C. F., 1980. Rhizoliths in terrestrial carbonates: classification, recognition, genesis and significance. *Sedimentology,* Volume 27, pp. 613-629.

Lifton, N., Sato, T. & Dunai, T. J., 2014. Scaling in situ cosmogenic nuclide production rates using analytical approximations to atmospheric cosmic-ray fluxes. *Earth and Planetary Science Letters,* Volume 386, pp. 149-160.

Lisiecki, L. E. & Raymo, M. E., 2005. A Pliocene-Pleistocene stack of 57 globally distributed benthic $\delta^{18}O$ records. *Paleoceanography,* Volume 20.

Marchetti, D. M., 2006. Quaternary geology of the Fremont River drainage basin, Utah. *PhD thesis,* pp. 1-186.

Marchetti, D. W., Cerling, T. E., Dohrenwend, J. C. & Gallin, W., 2007. Ages and significance of glacial and mass movement deposits on the west side of Boulder Mountain, Utah, USA. *Palaeogeogr Palaeoclim Palaeoecol,* Issue 252, pp. 503-513.

Marchetti, D. W., Hynek, S. A. & Cerling, T. E., 2012. Gravel-capped benches above northern tributaries of the Escalante River, south-central Utah. *Geosphere,* 8(4), pp. 835-853.

Marion, G. M., Verburg, P., Stevenson, B. & Arnone, J., 2008. Soluble element distributions in a Mojave Desert Soil. *Soil Sci. Soc. Am. J.,* 72(6), pp. 1815-1823.

McFadden, L. D., 2013. Strongly dust-influenced soils and what they tell us about landscape dynamics in vegetated aridlands of the southwestern United States. In: M. Bickford, ed. *The Web of Geological Sciences: Advances, Impacts, and Interactions.* s.l.:The Geological Society of America, pp. 501-532.

McFadden, L. D., Wells, S. G., Brown, W. J. & Enzel, Y., 1992. Soil genesis on beach ridges of pluvial lake Mojave: implications for Holocene lacustrine and eolian events in the Mojave Desert, southern California. *Catena,* Issue 19, pp. 77-97.

MesoWest, S. W. W. R., 2017. *CRN CAPITOL REEF NP 38.2898 -111.2619 1676 m SNOWNET.* [Online] Available at: http://mesowest.utah.edu/ [Accessed 14 April 2017].

Meyer, N. A., Breecker, D. O., Young, M. H. & Litvak, M. E., 2014. Simulating the effect of vegetation in formation of pedogenic carbonate. *Soil Science Society of America Journal,* 78(3), pp. 914-924.

Monger, H. C., Daugherty, L. A., Lindemann, W. C. & Liddell, C. M., 1991. Microbial precipitation of pedogenic calcite. *Geology,* Volume 19, pp. 997-1000.

Oerter, E. & Bowen, G., 2017. In situ monitoring of H and O stable isotopes in soil water reveals ecohydrologic dynamics in managed soil systems. *Ecohydrology.*

Oerter, E. J. & Amundson, R., 2016. Climate controls on spatial and temporal variations in the formation of pedogenic carbonate in the western Great Basin of North America. *GSA Bulletin,* pp. 1-10.

Oerter, E. J. et al., 2016. Pedothem carbonates reveal anomalous North American atmospheric circulation 70,000-55,000 years ago. *PNAS,* Volume 113, pp. 919-924.

Oerter, E., Perelet, A., Pardyjak, E. & Bowen, G., 2017. Membrane inlet laser spectroscopy to measure H and O stable isotope compositions of soil and sediment pore water with high sample throughput. *Rapid Communications in Mass Spectrometry,* Volume 31, pp. 75-84.

Passey, B. H. & Henkes, G. A., 2012. Carbonate clumped isotope bond reordering and geospeedometry. *Earth and Planetary Science Letters,* Volume 351-352, pp. 223-236.

Passey, B. H. et al., 2010. High temperature environments of human evolution from bond ordering in paleosol carbonates. *Proceedings of the National Academy of Sciences, USA,* Volume 107, pp. 11245-11249.

Pendall, E. et al., 2001. Elevated CO_2 stimulates soil respiration in a FACE wheat field. *Basic App. Ecol.,* Volume 2, pp. 193-201.

Peters, N. A., Huntington, K. W. & Hoke, G. D., 2013. Hot or not? Impact of seasonally variable soil carbonate formation on paleotemperature and O-isotope records from clumped isotope thermometry. *Earth and Planetary Science Letters,* Volume 361, pp. 208-218.

Prism Climate Group, 2018. *Oregon State University.* [Online]
Available at: http://prism.oregonstate.edu
[Accessed 26 January 2018].

Pustovoytov, K., Schmidt, K. & Taubald, H., 2007. Evidence for Holocene environmental changes in the Fertile Crescent provided by pedogenic carbonate coatings. *Quaternary Research,* Volume 67, pp. 315-327.

Quade, J., Eiler, J., Daëron, M. & Achyuthan, H., 2013. The clumped isotope geothermometer in soil and paleosol carbonate. *Geochimica et Cosmochimica Acta,* Volume 105, pp. 92-107.

Reheis, M. C. & Kihl, R., 1995. Dust deposition in southern Nevada and California, 1984-1989; relations to climate, source area, and source lithology. *J Geophys Res Atmos,* 100(D5), pp. 8893-8918.

Reimer, P. et al., 2009. IntCal09 and Marine09 radiocarbon age calibration curves, 0-50,000 years cal BP. *Radiocarbon,* Volume 51, pp. 1111-1150.

Ringham, M. C., Hoke, G. D., Huntington, K. W. & Aranibar, J. N., 2016. Influence of vegetation type and site-to-site variability on soil carbonate clumped isotope records, Andean piedmont of Central Argentina (32-34°S). *Earth and Planetary Science Letters,* Volume 440, pp. 1-11.

Romanek, C. S., Grossman, E. L. & Morse, J. W., 1992. Carbon isotopic fractionation in synthetic aragonite and calcite: Effects of temperature and precipitation rate. *Geochimica et Cosmochimica Acta,* Volume 56, pp. 419-430.

Schauble, E. A., Ghosh, P. & Eiler, J. M., 2006. Preferential formation of ^{13}C–^{18}O bonds in carbonate minerals, estimated using first-principles lattice dynamics. *Geochimica,* Volume 70, pp. 2510-2529.

Sharp, Z., 2007. *Principles of Stable Isotope Geochemistry.* 1st ed. Upper Saddle River, NJ: Pearson Education, Inc.

Snell, K. E. et al., 2013. Hot summers in the Bighorn Basin during the early Paleogene. *Geology,* Volume 41, pp. 55-58.

Solomon, D. K. & Cerling, T. E., 1987. The annual carbon dioxide cycle in a montane soil: observations, modeling, and implications for weathering. *Water Resources Research,* 23(12), pp. 2257-2265.

Stuvier, M. & Reimer, R. W., 1993. Extended ^{14}C database and revised CALIB radiocarbon calibration program. *Radiocarbon,* Volume 35, pp. 215-230.

Suarez, D. L., 1977. Ion activity products of calcium carbonate in waters below the root zone. *Soil. Ci. Soc. Am. J.,* 41(2), pp. 310-315.

Tipple, B. J. & Pagani, M., 2007. The early origins of terrestrial C_4 photosynthesis. *Annu. Rev. Earth Planet. Sci.,* Issue 35, pp. 435-461.

Treadwell-Steitz, C. & McFadden, L. D., 2000. Influence of parent material and grain size on carbonate coatings in gravelly soils, Palo Duro Wash, New Mexico. *Geoderma,* Issue 94, pp. 1-22.

Zhu, T. & Dittrich, Z., 2016. Carbonate precipitation through microbial activities in natural environment, and their potential in biotechnology: A Review. *Frontiers in Bioengineering and Biotechnology,* Volume 4, pp. 1-21.

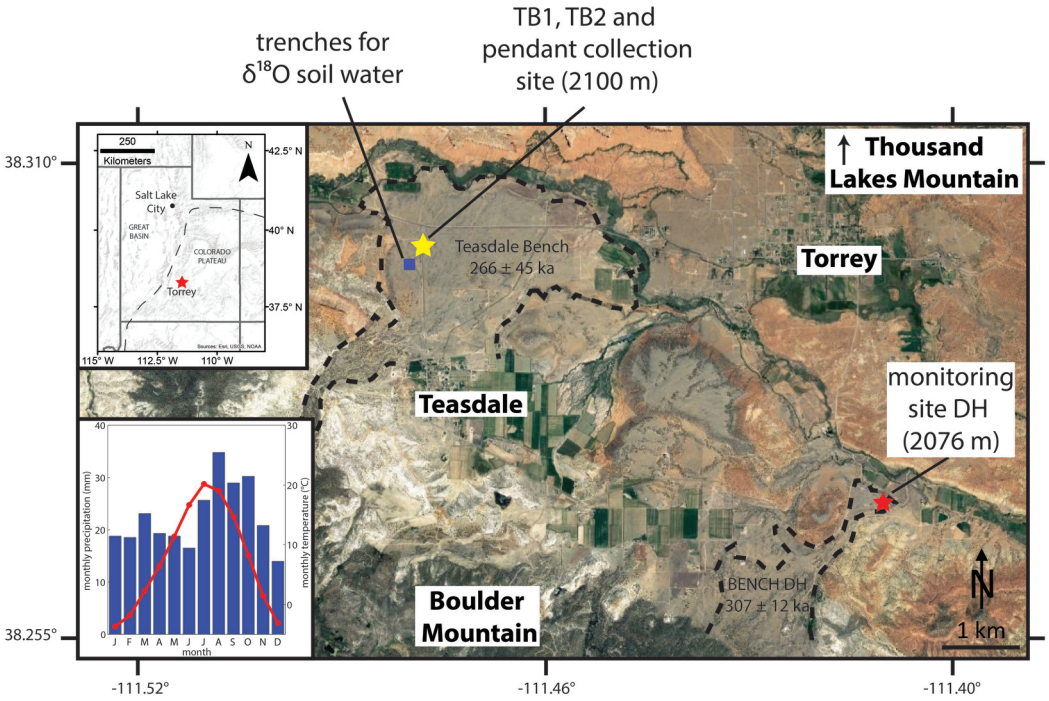

2018JG004496-f01-z-.jpg

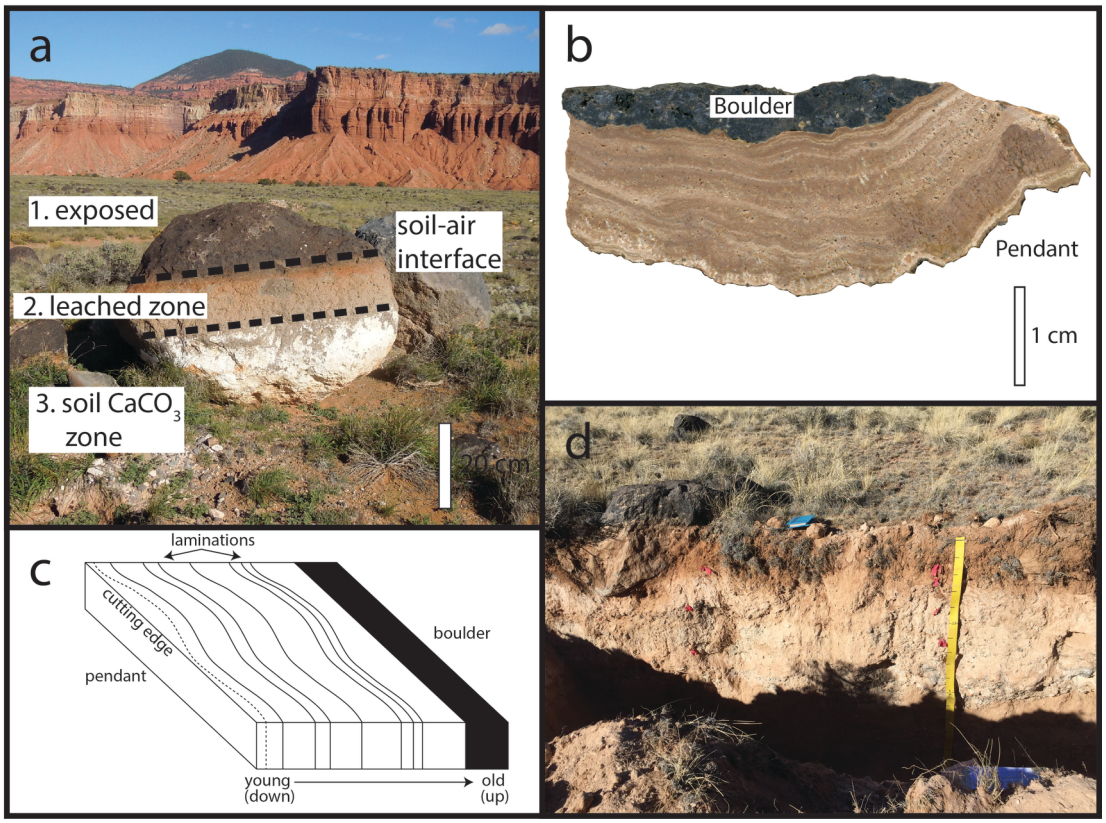

2018JG004496-f02-z-.jpg

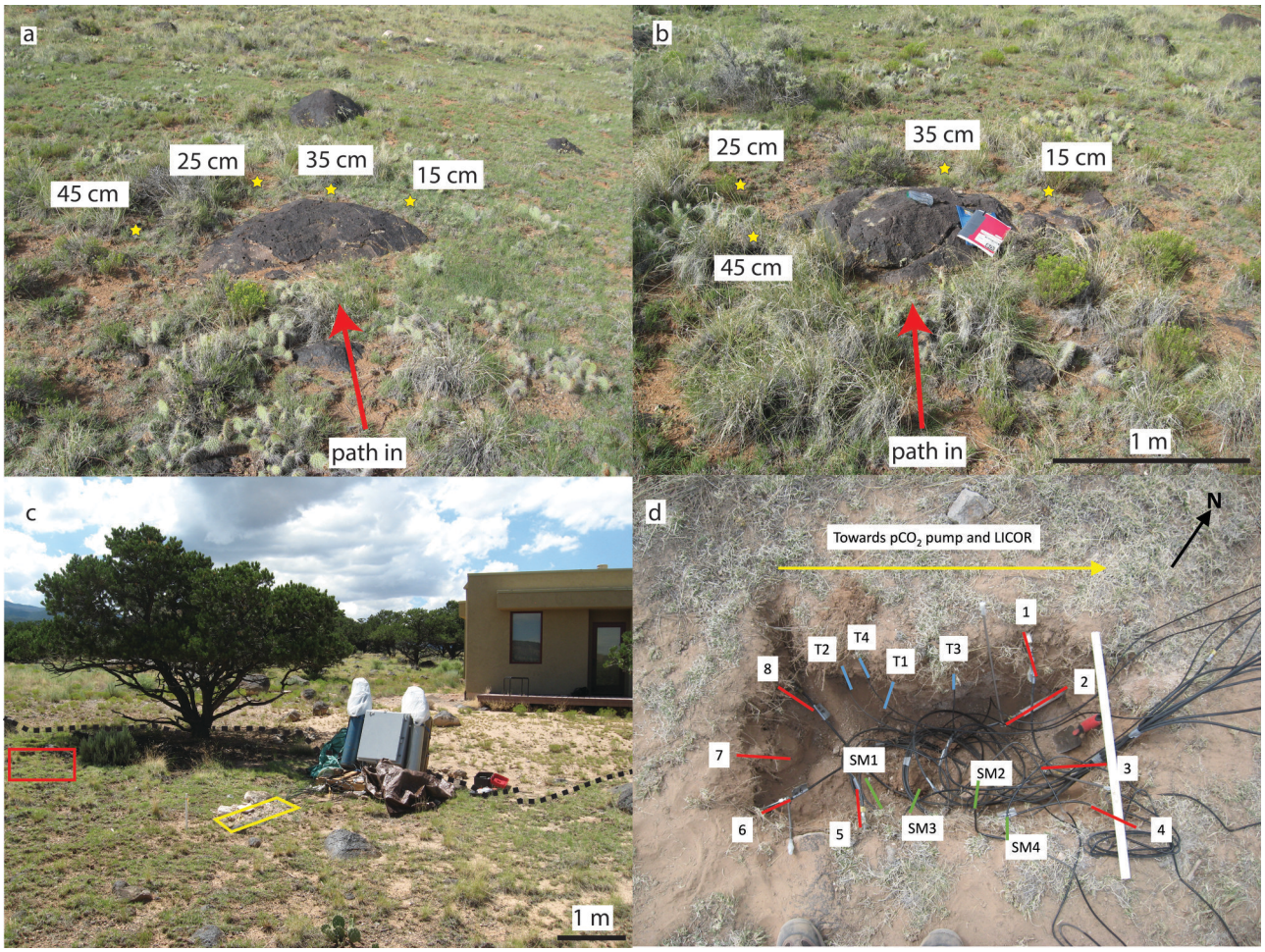

2018JG004496-f03-z-.jpg

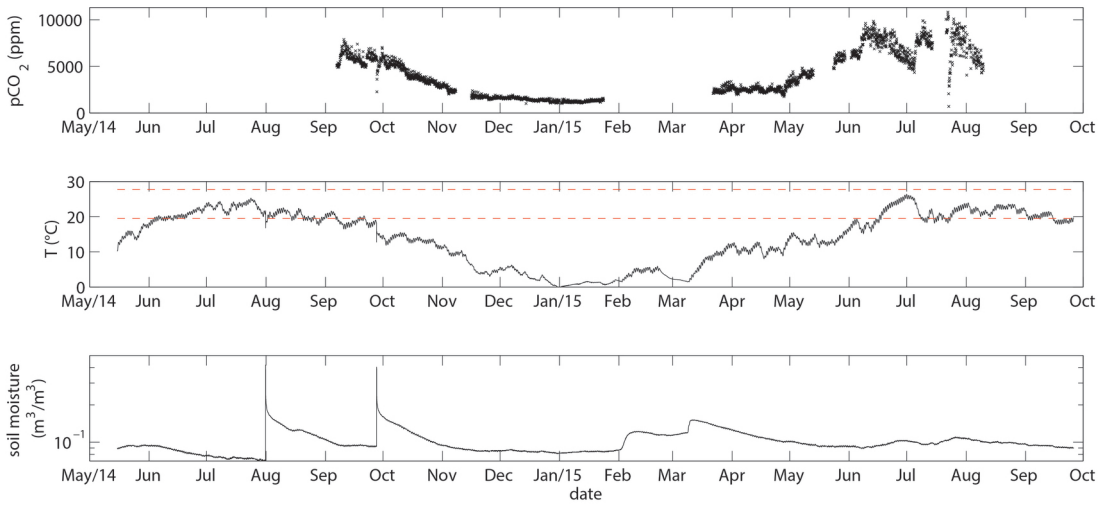

2018JG004496-f04-z-.jpg

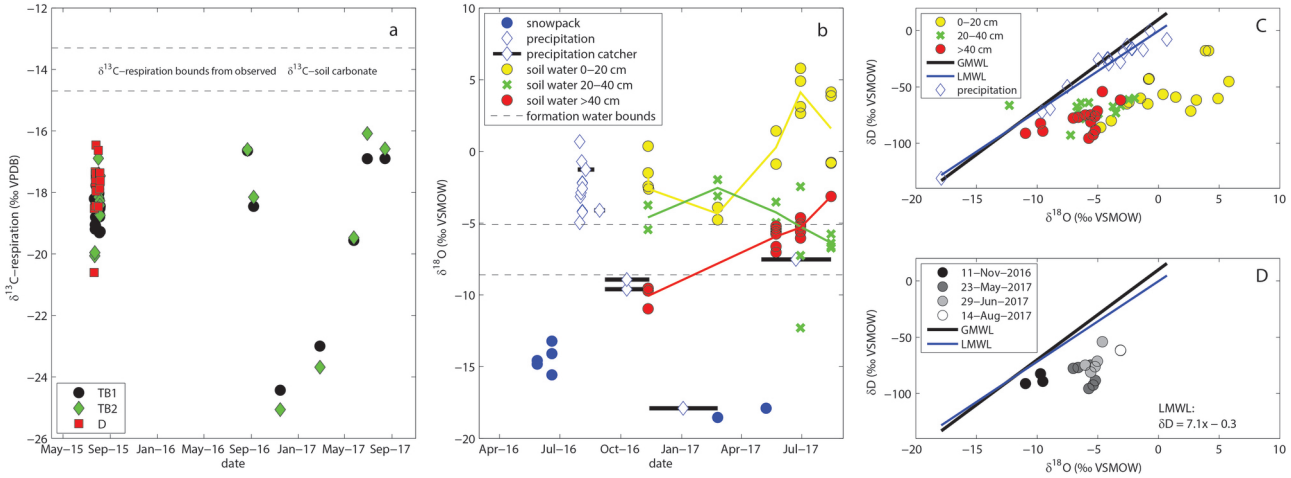

2018JG004496-f05-z-.jpg

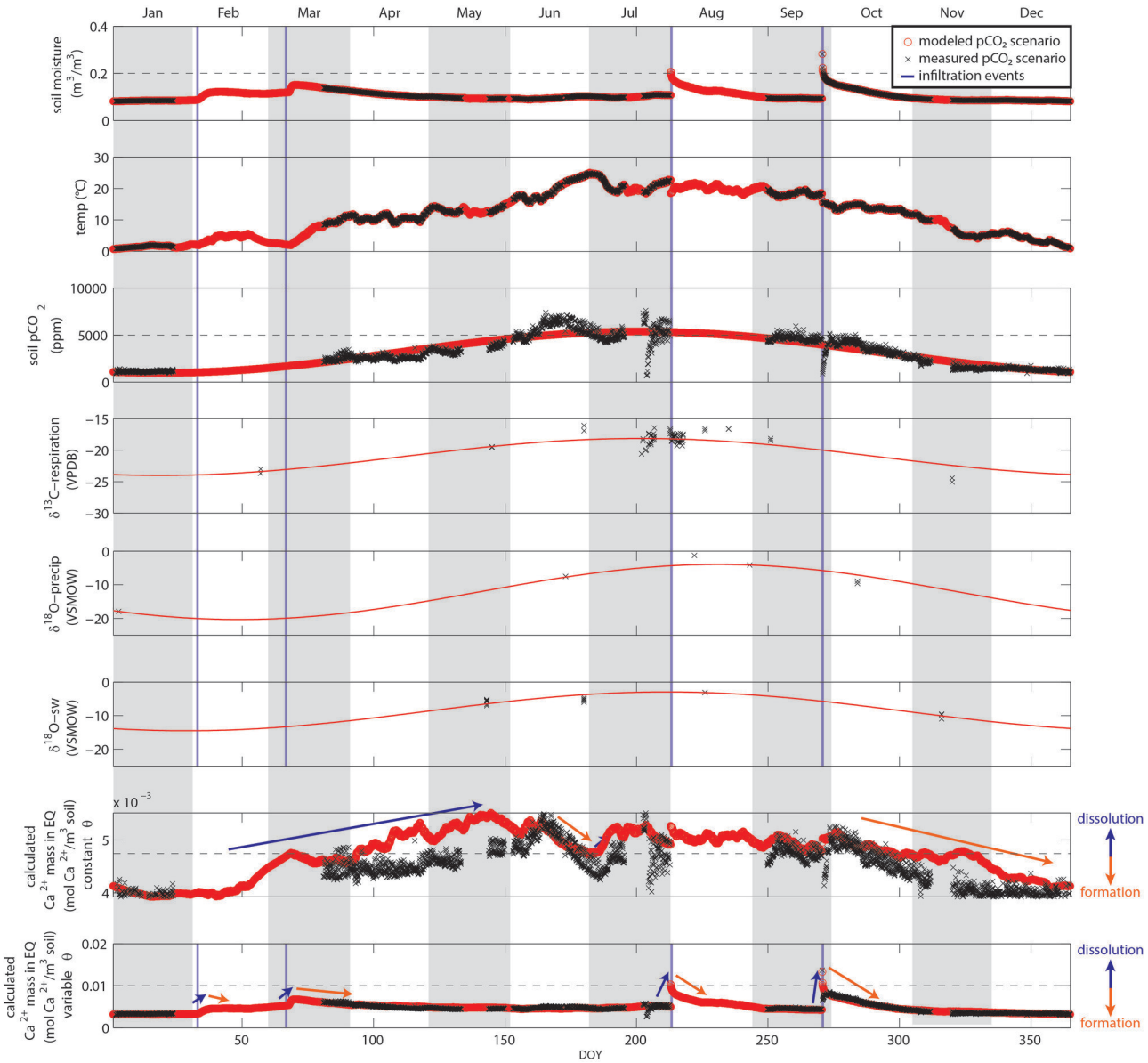

2018JG004496-f06-z-.jpg